Zero-temperature phase transitions and their anomalous influence on thermodynamic behavior in the q-state Potts model on a diamond chain

Yury Panov
Department of Theoretical and Mathematical Physics, Institute of Natural Sciences and Mathematics, Ural Federal University, 19 Mira Street, 620002 Ekaterinburg, Russia

Onofre Rojas
Department of Physics, Institute of Natural Science, Federal University of Lavras, 37200-900 Lavras, Minas Gerais, Brazil

(Received 27 July 2023; accepted 5 October 2023; published 26 October 2023)

The q-state Potts model on a diamond chain has mathematical significance in analyzing phase transitions and critical behaviors in diverse fields, including statistical physics, condensed matter physics, and materials science. By focusing on the three-state Potts model on a diamond chain, we reveal rich and analytically solvable behaviors without phase transitions at finite temperatures. Upon investigating thermodynamic properties such as internal energy, entropy, specific heat, and correlation length, we observe sharp changes near zero temperature. Magnetic properties, including magnetization and magnetic susceptibility, display distinct behaviors that provide insights into spin configurations in different phases. However, the Potts model lacks genuine phase transitions at finite temperatures, in line with the Peierls argument for one-dimensional systems. Nonetheless, in the general case of an arbitrary q state, magnetic properties such as correlation length, magnetization, and magnetic susceptibility exhibit intriguing remnants of a zero-temperature phase transition at finite temperatures. Furthermore, residual entropy uncovers unusual frustrated regions at zero-temperature phase transitions. This feature leads to the peculiar thermodynamic properties of phase boundaries, including a sharp entropy change resembling a first-order discontinuity without an entropy jump, and pronounced peaks in second-order derivatives of free energy, suggestive of a second-order phase transition divergence but without singularities. This unusual behavior is also observed in the correlation length at the pseudocritical temperature, which could potentially be misleading as a divergence.

DOI: 10.1103/PhysRevE.108.044144

I. INTRODUCTION

The one-dimensional Potts model, while simpler than higher-dimensional models, exhibits a range of intriguing properties making it a focus of study. It can often be solved exactly, offering valuable insight into statistical systems without the need for approximations or numerical methods [1]. These models lay the groundwork for understanding more complex behaviors in higher dimensions and are central to the study of phenomena like phase transitions in statistical physics [2]. They can represent a variety of physical and mathematical systems, such as counting colored planar map problems [3]. Additionally, they provide a practical platform for testing new computational methods, including Monte Carlo algorithms and machine learning techniques applied to statistical physics [4].

Even though a finite-temperature phase transition is absent in one-dimensional models with short-range interaction, it is still feasible to define and study a pseudocritical temperature. This is commonly perceived as the temperature at which a system fluctuation reaches a peak, often associated with the system specific heat, which generally exhibits a peak at the pseudocritical temperature. In this sense, recent research has unveiled a series of decorated one-dimensional models, notably the Ising and Heisenberg models, each exhibiting a range of structures. Among these are the Ising-Heisenberg diamond chain [5,6], the one-dimensional double-tetrahedral model with a nodal site comprising a localized Ising spin alternating with a pair of mobile electrons delocalized within a triangular plaquette [7], the ladder model with an Ising-Heisenberg coupling in alternation [8], and the triangular tube model with Ising-Heisenberg coupling [9]. Pseudotransition phenomena were detected in all these models. While the first derivative of the free energy, like entropy, internal energy, or magnetization, demonstrates a jump akin to an abrupt change when the temperature varies, the function remains continuous. This pattern mimics a first-order phase transition. Nevertheless, a second-order derivative of free energy, such as the specific heat and magnetic susceptibility, showcases behavior typical of a second-order phase transition at a finite temperature. This peculiar behavior has drawn attention for a more meticulous study, as discussed in Ref. [10]. More recently, Ref. [11] has provided additional discussion of this property and an exhaustive study of the correlation function for arbitrarily distant spins surrounding the pseudotransition. Furthermore, certain conditions were proposed to observe the pseudotransition, which is associated with residual entropy [12,13].

Recent discoveries have positioned azurite $[Cu_3(CO_3)_2(OH)_2]$ as an intriguing quantum antiferromagnetic model, as described by the Heisenberg model on a diamond chain. This has led to numerous riveting theoretical investigations into diamond chain models. Notably, Honecker *et al.* [14] probed the dynamic and thermodynamic traits of this model, while comprehensive analysis was conducted on the thermodynamic attributes of the Ising-Heisenberg model on diamondlike chains [15–19]. Additional studies into the Ising XYZ diamond chain model were inspired by current research, including experimental explorations of the natural mineral azurite and theoretical calculations of the Ising XXZ model. Particular attention was drawn by the appearance of a $\frac{1}{3}$ magnetization plateau and a double peak in both magnetic susceptibility and specific heat in experimental measurements [20–22]. It is relevant to note that the dimer interactions (interstitial sites) exhibit considerably stronger exchange interaction than the nodal sites on x and y axes, especially in the z component. Consequently, this model can be accurately represented as an exactly solvable Ising-Heisenberg model. Further supporting this, experimental data regarding the magnetization plateau align with the approximated Ising-Heisenberg model [15,23,24].

In the context of one-dimensional Potts models, Sarkanych *et al.* [25] introduced a variation featuring invisible states and short-range coupling. The notion of invisible in this context refers to an additional level of energy degeneracy that contributes solely to entropy without affecting interaction energy, thus catalyzing the first-order phase transition. This proposal was inspired by low-dimensional systems such as the simple zipper model [26], a descriptor of long-chain DNA nucleotides. To account for narrow helix-coil transitions within these systems, Zimm and Bragg [26] put forth a largely phenomenological cooperative parameter. This innovative approach has since sparked numerous inquiries [27–30]. In one-dimensional cooperative systems, Potts-like models [27,29] serve as an effective representation, providing a study of helix-coil transitions in polypeptides [28], a classic application of theoretical physics to macromolecular systems, yielding insightful comprehension of helix-coil transition properties. The reversible adsorption demonstrated by polycyclic aromatic surface elements in carbon nanotubes (CNTs) and aromatic DNA further enriches these studies. To consider DNA-CNT interactions, Tonoyan *et al.* [30] adjusted the Hamiltonian of the zipper model [26]. Similarly, our earlier work [31] proposed a one-dimensional Potts model combined with the Zimm-Bragg model, which we call here simply the Potts-Zimm-Bragg model, leading to the observation of several distinctive properties.

The paper is structured as follows. Section II presents our proposal for a q-state Potts model on a diamond chain structure. Section III analyzes the zero-temperature phase transition, residual entropy, and corresponding magnetizations. Section IV discusses the thermodynamic solution for finite-q states and explores physical quantities such as entropy, magnetization, specific heat, magnetic susceptibility, and correlation length. This section also highlights the presence of pseudocritical temperatures. Section V summarizes our findings and draws conclusions. Some details of the methods used, such as the decoration transformation and the application of Markov chain theory, are given in the Appendixes.

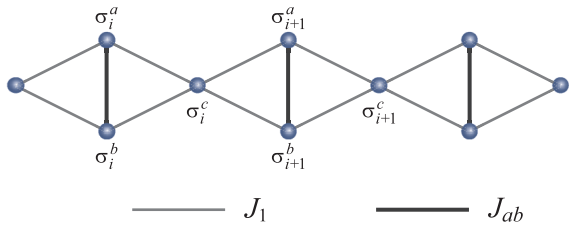

FIG. 1. Schematic representation of the Potts model on the diamond chain structure.

II. POTTS MODEL ON A DIAMOND CHAIN

Despite the simplicity of the one-dimensional Potts model, it possesses several intriguing properties that render it a worthy subject of study. With this in mind, consider a q-state Potts model on a diamond chain structure, as depicted in Fig. 1. The unit cell in this model is composed of three types of spins: two dimer spins σ_a and σ_b, interconnected by the coupling parameter J_{ab}, and a nodal spin σ_c, interacting with the dimer spins through the parameter J_1. The corresponding Potts Hamiltonian, based on this setup, can be articulated as

$$H = -\sum_{i=1}^{N}\Big[J_{ab}\delta_{\sigma_i^a,\sigma_i^b} + h_1\delta_{\sigma_i^c,1} + h_2\big(\delta_{\sigma_i^a,1} + \delta_{\sigma_i^b,1}\big) + J_1\big(\delta_{\sigma_i^c,\sigma_i^a} + \delta_{\sigma_i^c,\sigma_i^b} + \delta_{\sigma_i^c,\sigma_{i+1}^a} + \delta_{\sigma_i^c,\sigma_{i+1}^b}\big)\Big], \tag{1}$$

where $\sigma = \{1, \ldots, q\}$.

It is noteworthy that the Hamiltonian (1) can be mapped onto an effective one-dimensional Potts-Zimm-Bragg model [31], as detailed in Appendix A. This suggests that the Potts model on a diamond chain can be equated to a bona fide one-dimensional Potts-Zimm-Bragg model as studied in Ref. [31]. It should be noted, however, that the effective parameters of the effective Potts-Zimm-Bragg model now depend on temperature.

Transfer matrix of the q-state Potts model

In what follows we will focus our attention on the thermodynamics properties; to obtain the partition function we will use the standard transfer matrix technique. After obtaining each elements of the transfer matrix, the q-dimension transfer matrix elements have the structure

$$V = \begin{pmatrix} d_1 & t_1 & t_1 & \cdots & t_1 & t_1 \\ t_1 & d_2 & t_2 & \cdots & t_2 & t_2 \\ t_1 & t_2 & d_2 & \cdots & t_2 & t_2 \\ \vdots & \vdots & \vdots & \ddots & \vdots & \vdots \\ t_1 & t_2 & t_2 & \cdots & d_2 & t_2 \\ t_1 & t_2 & t_2 & \cdots & t_2 & d_2 \end{pmatrix}. \tag{2}$$

Therefore, let us write the transfer matrix eigenvalues similarly to those defined in Ref. [10], whose eigenvalues become

$$\lambda_1 = \tfrac{1}{2}\big[w_1 + w_{-1} + \sqrt{(w_1 - w_{-1})^2 + 4w_0^2}\big], \quad (3)$$

$$\lambda_2 = \tfrac{1}{2}\big[w_1 + w_{-1} - \sqrt{(w_1 - w_{-1})^2 + 4w_0^2}\big], \quad (4)$$

$$\lambda_j = (d_2 - t_2), \quad j = \{3, 4, \ldots, q\}, \quad (5)$$

where the elements are expressed as

$$w_1 = d_1, \quad (6)$$

$$w_{-1} = d_2 + (q-2)t_2, \quad (7)$$

$$w_0 = \sqrt{q-1}\, t_1, \quad (8)$$

considering the notation

$$d_1 = z_1\big[(q - 1 + x^2 z_2)^2 + (y-1)\big(q - 1 + x^4 z_2^2\big)\big], \quad (9)$$

$$d_2 = (q - 2 + x^2 + z_2)^2 + (y-1)\big(q - 2 + x^4 + z_2^2\big), \quad (10)$$

$$t_1 = \sqrt{z_1}[q - 2 + x(z_2 + 1)]^2 + \sqrt{z_1}(y-1)\big[q - 2 + x^2\big(z_2^2 + 1\big)\big], \quad (11)$$

$$t_2 = (q - 3 + 2x + z_2)^2 + (y-1)\big(q - 3 + 2x^2 + z_2^2\big), \quad (12)$$

where we used the notation $x = e^{\beta J_1}$, $y = e^{\beta J_{ab}}$, $z_1 = e^{\beta h_1}$, and $z_2 = e^{\beta h_2}$. We can also obtain the corresponding transfer matrix eigenvectors, which are given by

$$|u_1\rangle = \cos(\phi)|1\rangle + \frac{\sin(\phi)}{\sqrt{q-1}} \sum_{\mu=2}^{q} |\mu\rangle, \quad (13)$$

$$|u_2\rangle = -\sin(\phi)|1\rangle + \frac{\cos(\phi)}{\sqrt{q-1}} \sum_{\mu=2}^{q} |\mu\rangle, \quad (14)$$

$$|u_j\rangle = \sqrt{\frac{j-2}{j-1}}\left(\frac{1}{j-2}\sum_{\mu=2}^{j-1}|\mu\rangle - |j\rangle\right), \quad j = \{3, \ldots, q\}, \quad (15)$$

where $\phi = \frac{1}{2}\cot^{-1}(\frac{w_1 - w_{-1}}{2w_0})$, with $-\frac{\pi}{4} \leqslant \phi \leqslant \frac{\pi}{4}$.

By using the transfer matrix eigenvalues, we express the partition function as

$$Z_N = \lambda_1^N + \lambda_2^N + (q-2)\lambda_3^N = \lambda_1^N\left[1 + \left(\frac{\lambda_2}{\lambda_1}\right)^N + (q-2)\left(\frac{\lambda_3}{\lambda_1}\right)^N\right]. \quad (16)$$

It is evident that the eigenvalues satisfy the relation $\lambda_1 > \lambda_2 \geqslant \lambda_3$. Hence, assuming q is finite, the free energy in thermodynamic limit ($N \to \infty$) reduces to

$$f = -T\ln(\lambda_1). \quad (17)$$

It is important to acknowledge that the free energy for any finite-q state presents a continuous function, without any singularities or discontinuities. As a result, we should not anticipate any genuine phase transition at a finite temperature.

Furthermore, we can also compute the free energy (17) from the effective one-dimensional Potts-Zimm-Bragg model [31]. The specifics of this mapping are outlined in Appendix A. Note that the effective parameters of the Potts-Zimm-Bragg model are temperature dependent.

III. ZERO-TEMPERATURE PHASE DIAGRAM

In order to describe the ground state of the q-state Potts model on a diamond chain we use the following notation for the state of ith unit cell:

$$\big|\big[{}^{\mu_i}_{\nu_i}\big]\alpha_i\big\rangle_i = \big\{\big|{}^{\mu_i}_{\nu_i}\alpha_i\big\rangle_i \text{ or } \big|{}^{\nu_i}_{\mu_i}\alpha_i\big\rangle_i\big\}. \quad (18)$$

Here μ_i, ν_i, and α_i stand for the states of sites a, b, and c in the ith unit cell and the square brackets inside a ket vector denote two equivalent configurations for the values of Potts spins on a and b sites. Assuming $q \geqslant 3$ in Hamiltonian (1), we identify the ground states

$$|\mathrm{FM}_1\rangle = \prod_i \big|{}^1_1 1\big\rangle_i, \quad |\mathrm{FM}_2\rangle = \prod_i \big|{}^\mu_\mu \mu\big\rangle_i, \quad (19)$$

$$|\mathrm{FR}_1\rangle = \prod_i \big|{}^1_1 \mu_i\big\rangle_i, \quad |\mathrm{FR}_2\rangle = \prod_i \big|\big[{}^1_{\mu_i}\big]1\big\rangle_i, \quad (20)$$

$$|\mathrm{FR}_3\rangle = \prod_i \big|\big[{}^{\mu_i}_{\nu_i}\big]\mu_i\big\rangle_i, \quad |\mathrm{FR}_4\rangle = \prod_i \big|{}^{\nu_i}_{\nu_i}\mu_i\big\rangle_i, \quad (21)$$

$$|\mathrm{FR}_5\rangle = \prod_i \big|\big[{}^{\mu_i}_{\nu_i}\big]1\big\rangle_i, \quad |\mathrm{FR}_6\rangle = \prod_i \big|\big[{}^1_{\nu_i}\big]\mu_i\big\rangle_i, \quad (22)$$

$$|\mathrm{FR}_7\rangle = \prod_i \big|\big[{}^{\xi_i}_{\nu_i}\big]\mu_i\big\rangle_i. \quad (23)$$

Here the state indices μ, ν, and ξ are in a range $2, \ldots q$ and are not equal to each other if they are written in the same ket vector. The cell index i indicates that the site states in neighboring cells can differ, so for the frustrated phases the ground state consists of all relevant combinations and has nonzero residual entropy.

Expressions for energy and entropy per unit cell for the ground states (19)–(23) are given in Table I. It is important to note that the internal energy at zero temperature does not depend on q, while the residual entropy is completely determined by q. The frustrated phases are numbered in order of increasing residual entropy for $q \geqslant 7$. The dependence on q of the residual entropy for different phases is shown in Fig. 2.

The ground-state phase diagrams assuming that $h_1 = h_2 = h$ are shown in Figs. 3(a)–3(f) in different planes. The states $\mathrm{FM}_{1,2}$ are of the pure ferromagnetic type. The FM_1 (FM_2) phase is realized if $h > 0$ ($h < 0$). In general, the phase FM_2 is a multidomain and it consists of $q-1$ kinds of equivalent macroscopic domains having all spins of a diamond chain in the μ state. The state FR_1 is the first of the frustrated-type states. The a and b spins are in a state 1, while c spins may be in any of $\mu_i = 2, \ldots, q$ states, so the FR_1 phase is realized only if $h > 0$ and $J_1 < 0$. The number of states of c spins determines the entropy of the phase, $\mathcal{S}_0 = \ln(q-1)$ per unit cell. In the second frustrated phase FR_2, the spin a equals $\mu = 2, \ldots, q$, and the two remaining spins in the unit cell equal 1, so this phase exists at $J_{ab} < 0$. Due to the equivalence of sites a and b, the entropy of the FR_2 phase is greater by $\ln 2$. Frustrated phases $\mathrm{FR}_{3,4,7}$ exist only if $h < 0$. In the FR_3 phase, the spin states in the unit cell do not equal 1. The state of the

TABLE I. Ground-state energy, residual entropy, and magnetizations of a diamond Potts chain.

Ground state	ε_0	$\mathcal{S}_0$	m_c	m_{ab}
FM_1	$-(4J_1+J_{ab}+3h)$	0	1	2
FM_2	$-(4J_1+J_{ab})$	0	0	0
FR_1	$-(J_{ab}+2h)$	$\ln(q-1)$	0	2
FR_2	$-(2J_1+2h)$	$\ln[2(q-1)]$	1	1
FR_3	$-2J_1$	$\ln[4(q-2)]$	0	0
FR_4	$-J_{ab}$	$2\ln(q-2)$	0	0
FR_5	$-h$	$\ln[(q-1)(q-2)]$	1	0
FR_6	$-h$	$\ln[2(q-2)^2]$	0	1
FR_7	0	$\ln[(q-2)(q-3)^2]$	0	0
FM_1-FM_2	$-(4J_1+J_{ab})$	0	$\frac{1}{q}$	$\frac{2}{q}$
FM_1-FR_1	$8J_1-J_{ab}$	$\ln(q)$	$\frac{1}{q}$	2
FR_1-FR_2	$-2(J_1+h)$	$\ln[2(q-1)]$	1	1
FM_1-FR_2	$2(J_1+J_{ab})$	$\ln(2q-1)$	1	$\frac{2q}{2q-1}$
FM_2-FR_3	$-2J_1$	$\ln(4q-7)$	0	0
FR_2-FR_3	$-2J_1$	$\ln[4(q-1)]$	$\frac{1}{q}$	$\frac{2}{q}$
FM_2-FR_4	$-2J_{ab}$	$2\ln(q-1)$	0	0
FR_1-FR_4	$-J_{ab}$	$2\ln(q-1)$	$\frac{1}{q}$	$\frac{2}{q}$
FR_1-FR_6	J_{ab}	$\ln(2q^2-7q+7)$	0	$\frac{2(q^2-3q+3)}{2q^2-7q+7}$
FR_2-FR_6	$2J_1$	$\ln\left\{\frac{1}{2}[3q^2-9q+8+\phi_1(q)]\right\}$[a]	$\frac{\phi_1(q)-q^2+7q-8}{2\phi_1(q)}$	$\frac{\phi_1(q)+q^2-3q+4}{2\phi_1(q)}$
FR_4-FR_7	0	$\ln[(q-2)(q^2-5q+7)]$	0	0
FR_6-FR_7	0	$\ln[(q-1)(q-2)^2]$	$\frac{1}{q}$	$\frac{2}{q}$
FR_3-FR_7	0	$\ln[(q-1)^2(q-2)]$	0	0
FM_1-FR_1-FR_2	$6J_1$	$\ln\left\{\frac{1}{2}[3q-2+\phi_2(q)]\right\}$[b]	$\frac{q+\phi_2(q)}{2\phi_2(q)}$	$\frac{3\phi_2(q)-q+2}{2\phi_2(q)}$
FR_1-FR_2-FR_6	$2J_1$	$\ln\left\{\frac{1}{2}[3q^2-8q+7+\phi_3(q)]\right\}$[c]	$\frac{\phi_3(q)-q^2+6q-7}{2\phi_3(q)}$	$\frac{2\{(q^2-2q+2)[q^2-7+\phi_3(q)]+10-2q\}}{\phi_3(q)[3q^2-8q+7+\phi_3(q)]}$
FM_1-FM_2-FR_2-FR_3	$-2J_1$	$\ln(4q-3)$	$\frac{1}{q}$	$\frac{2}{q}$
FR_1-FR_4-FR_6-FR_7	0	$\ln[(q-1)(q^2-3q+3)]$	$\frac{1}{q}$	$\frac{2}{q}$
FM_2-FR_3-FR_4-FR_7	0	$3\ln(q-1)$	0	0
FR_2-FR_3-FR_6-FR_7	0	$\ln[q^2(q-1)]$	$\frac{1}{q}$	$\frac{2}{q}$
O	0	$3\ln(q)$	$\frac{1}{q}$	$\frac{2}{q}$

[a] $\phi_1(q)=\sqrt{q(q^3+2q^2-15q+16)}$.
[b] $\phi_2(q)=\sqrt{q^2+4q-4}$.
[c] $\phi_3(q)=\sqrt{q^4+4q^3-30q^2+44q-15}$.

c spin and the state of one of the spins a or b are the same, $\sigma_i^c=\sigma_i^{(a,b)}$, but the states of spins a and b in the same unit cell are different, $\sigma_i^a\neq\sigma_i^b$, so this phase appears as a ground state only if $J_{ab}<0$. Formally, the number of states of an elementary cell is $2(q-1)(q-2)$. However, for the given phase, the state of the chain should look the same when moving along the chain from left to right or in the opposite direction. This mirror symmetry generates the restriction $\sigma_{i-1}^{(a,b)}=\sigma_i^c=\sigma_i^{(a,b)}$, so the total number of states per unit cell in the FR_3 phase is $4(q-2)$. In turn, for the FR_4 phase, the conditions $\sigma_{i-1}^{(a,b)}\neq\sigma_i^c$ and $\sigma_i^c\neq\sigma_i^{(a,b)}$ must be met, so the total number of states per unit cell decreases from $(q-1)(q-2)$ to $(q-2)^2$. Under the assumption $h_1=h_2$, the energies of the FR_5 and FR_6 phases are equal, and these states do not mix at the microscopic level, that is, the unit cells of these states cannot alternate in the chain. Formally, the chain state in the FR_6 phase region in Fig. 3 should be a phase separation consisting of macroscopic domains of the FR_5 and FR_6 phases. The entropy of the FR_5 phase is determined by the total number of states in the unit cell, that is, $(q-1)(q-2)$. In the FR_6 phase, the conditions $\sigma_{i-1}^{(a,b)}\neq\sigma_i^c\neq\sigma_i^{(a,b)}$ give $2(q-2)^2$ states instead of the formally possible $2(q-1)(q-2)$ states in the unit cell. Nevertheless, at $q>3$ the entropy of the FR_5 phase is less than the entropy of the FR_6 phase; therefore, the free energy of the FR_6 phase at any finite temperature is the lowest, and in the limit at $T\to 0$ we will have the FR_6 phase as the ground state. However, the FR_5 contributes to the state at the FR_2-FR_6 phase boundary. In the frustrated phase FR_7, all the spins in the unit cell are pairwise unequal and are not equal to 1, so formally the number of states of an elementary cell is $(q-1)(q-2)(q-3)$. The restriction $\sigma_{i-1}^c\neq\sigma_i^{(a,b)}$ reduces the total number of states per unit cell to the value $(q-2)(q-3)^2$. If $q\geqslant 7$, the entropy of the FR_7 phase has the highest value among the other ground-state phases.

The case $q=3$ is special; the corresponding phase diagram is shown in Fig. 4. If $q=3$, then the states of the FR_7 phase cannot be realized, since in this case there are only two different Potts spins with $q\neq 1$ for the three sites in the unit cell. The phase FR_7 is absent and its region in the phase diagram

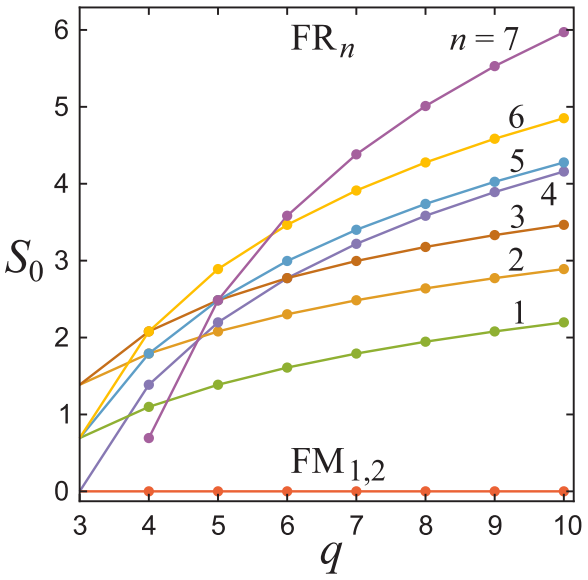

FIG. 2. Dependences on q of the residual entropy for different phases of the ground state (see Table I).

is taken by other phases. Also, the phase diagram contains both the FR_6 phase and the phase-separated state $FR_5 + FR_6$, which consist of equal fractions of the macroscopic domains of the phases FR_5 and FR_6. Both FR_6 and $FR_5 + FR_6$ phases and the boundary phase have the same entropy $\mathcal{S} = \ln 2$. The structure of the ground state here can be explored using the methods of the theory of Markov chains (see Appendix B).

To obtain the residual entropy $\mathcal{S}_0$ as a limit at zero temperature, we use equations for the internal energy ε and the free energy f,

$$\varepsilon = f + T\mathcal{S}, \quad f = -T\ln(\lambda_1), \tag{24}$$

where λ_1 is the maximum eigenvalue of the transfer matrix. Then

$$\mathcal{S} = \ln\left(\frac{\lambda_1}{e^{-\beta\varepsilon}}\right). \tag{25}$$

An explicit expression of λ_1 is given by Eq. (3) and we can write it in the form

$$\lambda_1 = e^{-\beta\varepsilon_0}\varphi(e^{-\beta(\varepsilon_1-\varepsilon_0)}, e^{-\beta(\varepsilon_2-\varepsilon_0)}, \ldots). \tag{26}$$

Here ε_0 is the ground-state energy for given parameters of the Hamiltonian, so relations $\varepsilon_k > \varepsilon_0$ are fulfilled for all k. The form of φ depends on the ground state. Since ε tends to ε_0 at zero temperature, we obtain

$$\mathcal{S}_0 = \ln[\varphi(0)]. \tag{27}$$

To find $\varphi(0)$, it is enough to zero out all exponential terms having $\varepsilon_k \neq \varepsilon_0$ and replace $e^{-\beta\varepsilon_0}$ by unity in λ_1.

A similar procedure can be defined for the magnetizations m_c and m_{ab} in the ground state. So, for the magnetizations m_c and m_{ab} we have the equations

$$m_c = \frac{1}{\lambda_1}\frac{\partial\lambda_1}{\partial(\beta h_1)}, \quad m_{ab} = \frac{1}{\lambda_1}\frac{\partial\lambda_1}{\partial(\beta h_2)}. \tag{28}$$

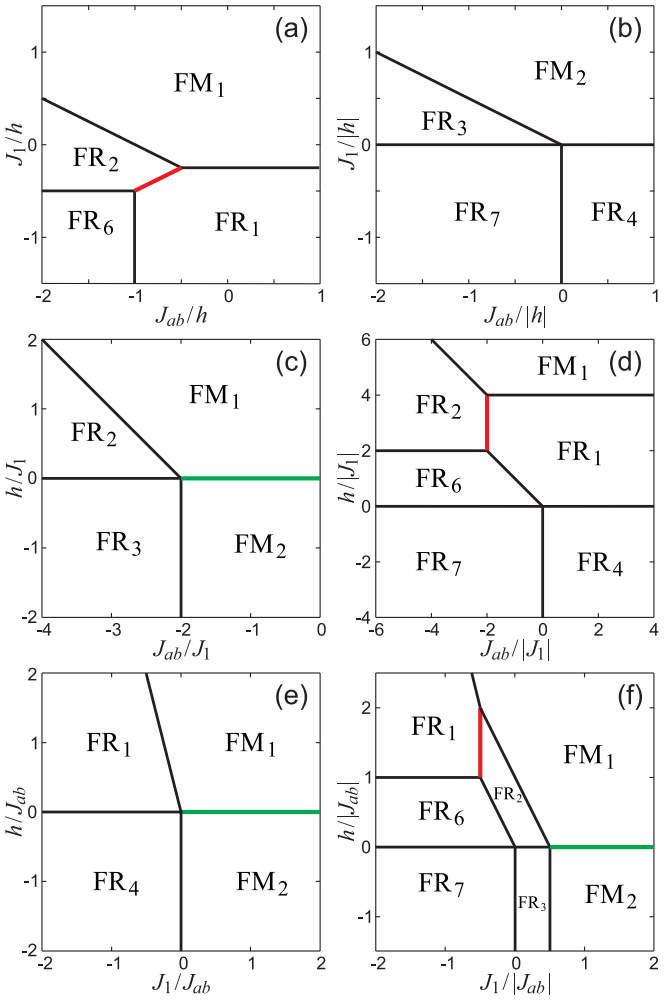

FIG. 3. Ground-state phase diagrams for the case $q > 3$ in the J_{ab}-J_1 plane for (a) $h > 0$ and (b) $h < 0$, in the J_{ab}-h plane for (c) $J_1 > 0$ and (d) $J_1 < 0$, and in the J_1-h plane for (e) $J_{ab} > 0$ and (f) $J_{ab} < 0$. The green lines show the FM_1-FM_2 boundaries where both adjacent phases and the boundary phase have zero entropy. The red lines are the FR_1-FR_2 boundaries, where $\mathcal{S}_{FR_1} < \mathcal{S}_{FR_1\text{-}FR_2} = \mathcal{S}_{FR_2}$.

If we define

$$\frac{\partial\lambda_1}{\partial(\beta h_1)} = e^{-\beta\varepsilon_0}\psi_c(e^{-\beta(\varepsilon_1-\varepsilon_0)}, e^{-\beta(\varepsilon_2-\varepsilon_0)}, \ldots), \tag{29}$$

$$\frac{\partial\lambda_1}{\partial(\beta h_2)} = e^{-\beta\varepsilon_0}\psi_{ab}(e^{-\beta(\varepsilon_1-\varepsilon_0)}, e^{-\beta(\varepsilon_2-\varepsilon_0)}, \ldots), \tag{30}$$

then in the ground state we get

$$m_c = \frac{\psi_c(0)}{\varphi(0)}, \quad m_{ab} = \frac{\psi_{ab}(0)}{\varphi(0)}. \tag{31}$$

The ground-state energy ε_0, the residual entropy $\mathcal{S}_0$, and magnetizations m_c and m_{ab}, which were found using Eqs. (27) and (31), are given in Table I for all phases and phase boundaries.

There is another way to get the values given in Table I and study the properties of the ground state in detail. This method, based on the theory of Markov chains, is described in Appendix B.

The values in Table I show that the entropy of all phase boundaries is greater than the entropy of adjacent phases.

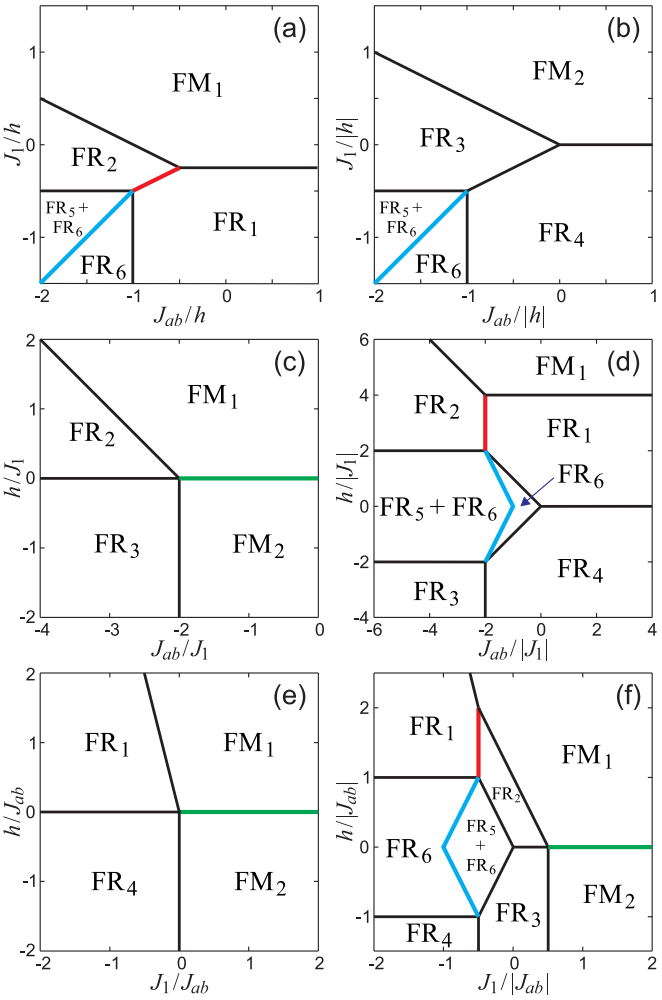

FIG. 4. Ground-state phase diagrams for the case $q = 3$ in the J_{ab}-J_1 plane for (a) $h > 0$ and (b) $h < 0$, in the J_{ab}-h plane for (c) $J_1 > 0$ and (d) $J_1 < 0$, and in the J_1-h plane for (e) $J_{ab} > 0$ and (f) $J_{ab} < 0$. The green lines show the FM_1-FM_2 boundaries where both adjacent phases and the boundary phase have zero entropy. The blue lines show the new boundaries between the FR_6 phase and the phase-separated state $FR_5 + FR_6$. The red lines are the FR_1-FR_2 boundaries, where $\mathcal{S}_{FR_1} < \mathcal{S}_{FR_1\text{-}FR_2} = \mathcal{S}_{FR_2}$.

The exceptions are two phase boundaries. The first is the FM_1-FM_2 boundary, where the entropy of both adjacent phases and the boundary state is zero. The second is the FR_1-FR_2 boundary, where the boundary state is such that $\mathcal{S}_{FR_1} < \mathcal{S}_{FR_1\text{-}FR_2} = \mathcal{S}_{FR_2}$. This phase boundary is truly an anomalous property, leading to a peculiar phase pseudotransition at finite temperature, which we will explore in the next section.

IV. THERMODYNAMICS OF THE q-STATE POTTS MODEL

In what follows, we will analyze the thermodynamic properties of the model in detail. First, we will examine the three-state models ($q = 3$), which exhibit some peculiar properties, distinct from the behavior for $q > 3$. Later, we will explore the case when $q > 3$. It is worth noting that the behavior for any $q > 3$ tends to be rather consistent across finite values of q. For the purposes of this discussion, we will focus specifically on $q = 5$, without losing its core properties.

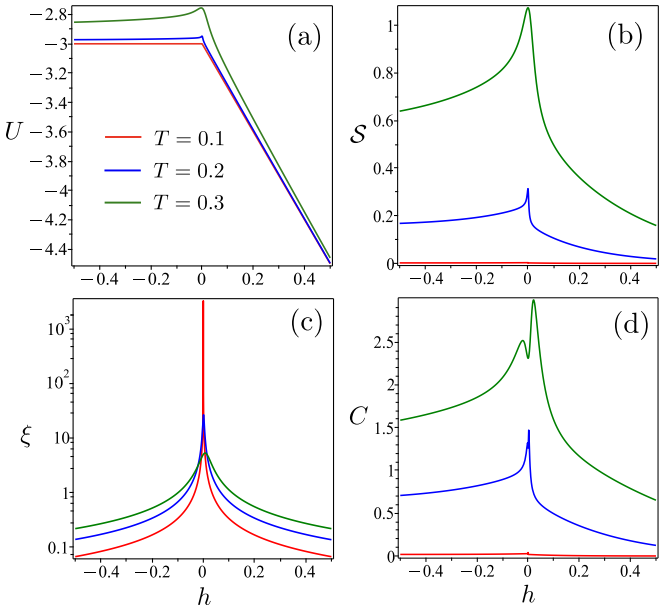

FIG. 5. (a) Internal energy U as a function of the external magnetic field, for three different temperature values $T = \{0.1, 0.2, 0.3\}$ assuming fixed parameters $J_{ab} = -1$, $J_1 = 1$, and $q = 3$. (b) Entropy $\mathcal{S}$ for the same conditions as in (a). (c) Correlation length. (d) Specific heat.

A. Three-state Potts model

Indeed, the two-state Potts model is equivalent to the Ising model, which differs significantly from the $q > 2$ state Potts model. A primary feature to highlight in the latter is the emergence of frustration. The three-state Potts model, being the first to exhibit this frustration behavior, is expected to display peculiar characteristics. In contrast, all higher-q-state Potts models tend to behave similarly. The one-dimensional three-state Potts model provides a richer set of behaviors than the two-state Ising model, yet it is still analytically solvable. Surely, in the one-dimensional case, there is no phase transition at finite temperature for the Potts model with $q > 2$ states, which can be proven via the Peierls argument [2]. This property makes the one-dimensional three-state Potts model a tractable system to study, helping investigations into more intricate systems and behaviors within statistical physics. Its study contributes to the broader field of statistical physics and has implications in several scientific disciplines. In this sense, here we will consider the special case of the three-state Potts model on a diamond chain.

Initially, we will explore the thermodynamics and magnetization properties in the vicinity of the zero-temperature phase boundary that separates FM_1 and FM_2. Figure 5(a) illustrates the internal energy U as a function of the external magnetic field. We assume the same magnetic field for both nodal and dimer sites ($h_1 = h_2 = h$). Three different temperature values are considered to demonstrate the behavior of the internal energy. At $h = 0$, corresponding to the zero-temperature phase transition between FM_1 and FM_2 (refer to Fig. 4), an evident

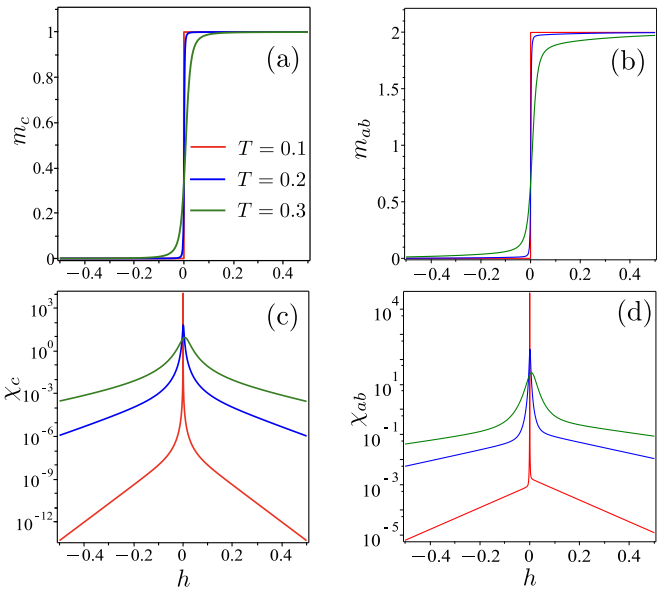

FIG. 6. (a) Magnetization m_c as a function of the external magnetic field h, for three different temperature values $T = \{0.1, 0.2, 0.3\}$, assuming fixed parameters $J_{ab} = -1$, $J_1 = 1$, and $q = 3$. (b) Magnetization m_{ab} as a function of the external magnetic field h, for the same set of fixed parameters as in (a). Magnetic susceptibilities (c) χ_c and (d) χ_{ab} are plotted assuming the same conditions as in (a) and (b).

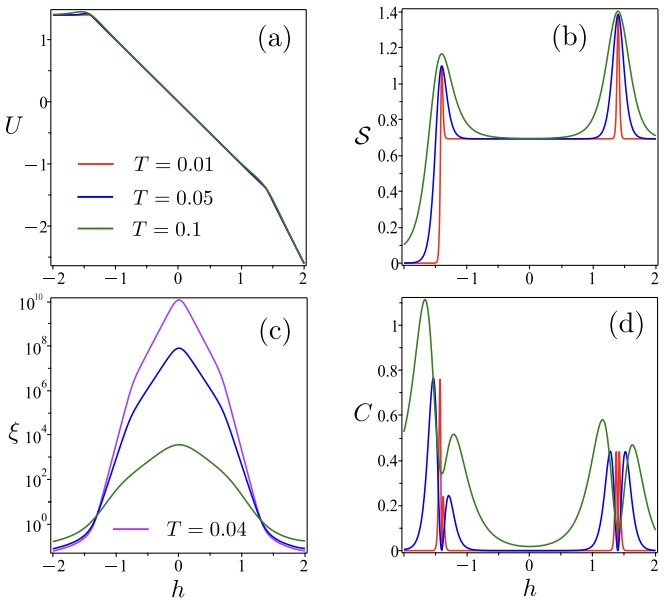

FIG. 7. (a) Internal energy U as a function of temperature for three specific values $T = \{0.01, 0.05, 0.1\}$, assuming fixed parameters $J_{ab} = -1.4$, $J_1 = -1$, and $q = 3$. (b) Entropy $\mathcal{S}$ under the same conditions as in (a). (c) Correlation length ξ. (d) Specific heat C.

change is observed. As the temperature increases, a small peak emerges at $h = 0$, which grows with higher temperatures. In Fig. 5(b) the entropy $\mathcal{S}$ is shown as a function of the external magnetic field, under the same conditions as in Fig. 5(a). Here we notice the absence of residual entropy at zero temperature, in accordance with the argument in Refs. [12,13], suggesting the presence of a pseudocritical temperature at this boundary. Figure 5(c) displays the correlation length $\xi = 1/\ln(\frac{\lambda_1}{\lambda_2})$ as a function of h, using the same parameter set as in Figs. 5(a) and 5(b). Once again, a sharp peak at $h = 0$ confirms the phase transition at zero temperature. Interestingly, in this case, there is not just one pseudocritical temperature but infinitely many. For any temperature $T_p \lesssim 0.2$, we observe a sharp peak in the correlation length at a null magnetic field. Finally, Fig. 5(d) presents the specific heat under the same conditions. In contrast to a typical pseudocritical peak, an intense peak appears, with a small minimum at $h = 0$. As the temperature decreases, the specific heat tends to zero, as expected.

In the following analysis, we explore the magnetic properties of the system, specifically the magnetization and magnetic susceptibility. Figure 6(a) illustrates the magnetization m_c of the nodal site as a function of the external magnetic field h for temperatures $T = \{0.1, 0.2, 0.3\}$. The parameters $J_{ab} = -1$ and $J_1 = 1$ remain fixed throughout. In the low-temperature region, we observe the saturated phase (FM_1) and a phase transition at $h = 0$, where the magnetization drops to zero, corresponding to FM_2. It is important to note that FM_2 exhibits null magnetization since, according to the definition in Eq. (20), it aligns in any state other than 1. Moving on to Fig. 6(b), we present the dimer magnetization m_{ab}, which exhibits behavior similar to that in Fig. 6(a). Figure 6(c) exhibits the magnetic susceptibility χ_c as a function of the external magnetic field h, under the same aforementioned conditions. Notably, it displays sharp peaks reminiscent of pseudocritical phase transitions, particularly for temperatures $T_p \lesssim 0.2$. Similarly, Fig. 6(d) illustrates the dimer magnetic susceptibility χ_{ab} as a function of h, employing the same conditions as in Figs. 6(a)–6(c). Figures 6(c) and 6(d) exhibit characteristic sharp peaks distinct from the double peak observed in the specific heat plot depicted in Fig. 5(d), which occurs around $h = 0$.

There is a peculiar behavior for $q = 3$, so we will now investigate the anomalous interface between FR_5 and $FR_5 + FR_6$, which represents another phase boundary that requires analysis. Figure 7(a) illustrates the internal energy U as a function of the external magnetic field h, with the parameters $J_{ab} = -1.4$ and $J_1 = -1$ held constant. The graph uses three distinct temperatures for illustrative purposes. The internal energies for these temperatures appear to be almost identical, with minor variations around $h = \pm 1.4$, where a zero-temperature phase transition occurs. In contrast, Fig. 7(b) depicts the entropy $\mathcal{S}$ as a function of the same set of temperatures. Unlike the internal energy, the entropies for these temperatures are distinctly different under the same set of parameters. A peak is noticeable at the same magnetic field $h = \pm 1.4$, underscoring the impact of the zero-temperature phase transition. On the other hand, the correlation length ξ indicates a curvature change at a disparate temperature, approximately around $h \approx \pm 0.8$, but no evidence of phase transition influence at $h = \pm 1.4$ is discernible. Finally, Fig. 7(d) demonstrates the specific heat as a function of temperature, maintaining the same parameters as in Fig. 7(a). A double peak is observable around $h = \pm 1.4$, but no signs of unusual behavior are evident at $h \approx \pm 0.8$. Although there is no anomalous behavior for U, $\mathcal{S}$, and C

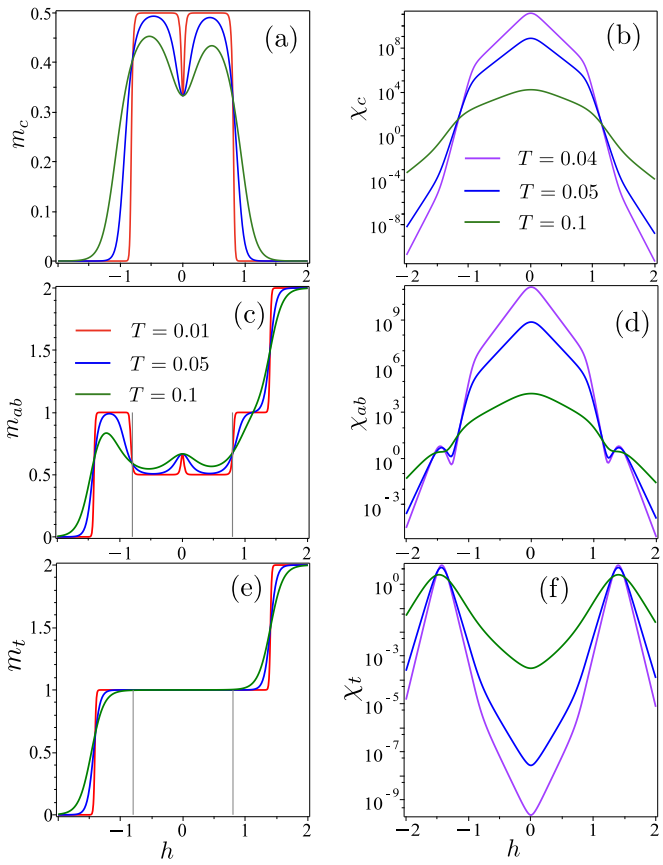

FIG. 8. (a) Magnetization m_c as a function of the external magnetic field h, considering three different temperature values $T = \{0.01, 0.05, 0.1\}$. The fixed parameters $J_{ab} = -1.4$, $J_1 = -1$, and $q = 3$ are assumed. (b) Magnetization m_{ab} as a function of the external magnetic field h, with the same set of fixed parameters as in (a). Magnetic susceptibilities (c) χ_c and (d) χ_{ab} are plotted under the same conditions as in (a) and (b).

at $h = 0$, the correlation length ξ illustrates a maximum at $h = 0$. This anomalous behavior will be further discussed later.

Figure 8(a) depicts the magnetization of nodal spin, assuming the same parameters as in Fig. 7. It reveals that the magnetization, denoted by m_c, alters its behavior notably at $h \approx \pm 0.8$. However, there are no traces of a phase transition at $h = \pm 1.4$, even though the magnetization exhibits symmetry under the exchange of the magnetic-field sign. Additionally, Fig. 8(b) reports the magnetic susceptibility χ_c of nodal spin, as a function of the magnetic field, with temperatures given in the legend. Note that the magnetic susceptibility increases rapidly for lower temperatures and remains substantial at $h = \pm 1$. It also displays a significant alteration in the curve around $h \approx \pm 0.8$ and a change in curvature at about $h \approx \pm 1.4$. In contrast, Fig. 8(c) illustrates the dimer magnetization, denoted by m_{ab}, as a function of the external magnetic field h. Here we observe the zero-temperature phase transition impact at $h = \pm 1.4$ and ± 0.8, despite the magnetization no longer maintaining symmetry under the exchange of the magnetic field. Similarly, Fig. 8(d) features the magnetic susceptibility χ_{ab}, using the same parameters presented in Fig. 8(a). Comparable to observations in Fig. 8(c), we detect a significant change of curvature around $h \approx \pm 0.8$, while a local maximum of magnetic susceptibility emerges at $h \approx \pm 1.4$. As previously identified in the correlation length ξ, there is an anomalous behavior observed at $h = 0$. The magnetization m_c exhibits a peculiar value of $\frac{1}{3}$ at null magnetic field, while similarly m_{ab} yields $\frac{2}{3}$ at $h = 0$, and obviously the total magnetization becomes 1. This anomalous behavior is also manifested in the magnetic susceptibilities χ_c and χ_{ab}, which exhibit a maximum value at $h = 0$ when the magnetic field is varied. Furthermore, in Fig. 8(e) we report the total magnetization $m_t = m_c + m_{ab}$. Interestingly, based on our observations, there is no evidence of any anomalous behavior; instead, a long plateau is evident. For this analysis, we assume the same set of parameters as those used for the previous partial magnetizations. Figure 8(f) shows the total magnetic susceptibility $\chi_t = \chi_c + \chi_{ab} + 2\chi_{abc}$, where $\chi_{abc} = -\frac{\partial^2 f}{\partial h_c \partial h_{ab}}$ (not depicted). Again, we rely on the parameters established for the partial magnetic susceptibilities. It is noteworthy that this analysis does not reveal significant insights around the anomalous regions. Additionally, the total magnetic susceptibility presents a markedly smaller magnitude compared to the partial magnetic susceptibilities displayed in Figs. 8(b) and 8(d). This reduced magnitude arises because the magnetic susceptibility χ_{abc} counterbalances the positive contributions from χ_c and χ_{ab}, due to its comparable magnitude. As an alternative approach, one can determine χ_t for the current case by assuming $h_c = h_{ab}$ and taking the second derivative of the negative free energy.

B. Pseudocritical temperature around the FR_1-FR_2 phase boundary

We will now investigate the properties of the Potts model on a diamond structure, which displays anomalous behavior near the FR_1-FR_2 phase boundary influenced by temperature variations. This region displays a pseudocritical transition, akin to a first- or second-order phase transition. Notably, the anomalous properties observed in the low-temperature regime are primarily independent of the particular value of q. For $q > 3$, the behavior of physical quantities is rather similar. Therefore, we will consider $q = 5$ solely for illustrative purposes, without losing any relevant properties. Examining this transition is crucial for comprehending the physical properties of the Potts model and predicting its behavior under diverse conditions.

1. Entropy

Figure 9(a) shows the plot of entropy $\mathcal{S}$ as a function of temperature T/T_p, where T_p is the pseudocritical temperature, with $J_{ab} = -0.75$, $J_1 = -0.38$, and $q = 5$ fixed parameters. We consider several magnetic fields, i.e., $h = \{0.8, 0.9, 1.0, 1.3, 1.4, 1.45\}$, and their corresponding pseudocritical temperatures are $T_p = \{0.010\,065\,153\,487\,1,\ 0.014\,347\,308\,824\,4,\ 0.014\,426\,811\,788\,3,\ 0.014\,426\,897\,057\,9,\ 0.014\,398\,249\,768\,6,\ 0.013\,983\,016\,139\,5\}$, respectively. For magnetic fields in the range of $1 \lesssim h \lesssim 1.3$, we observe a robust change of curvature at T_p, which resembles a typical first-order phase transition.

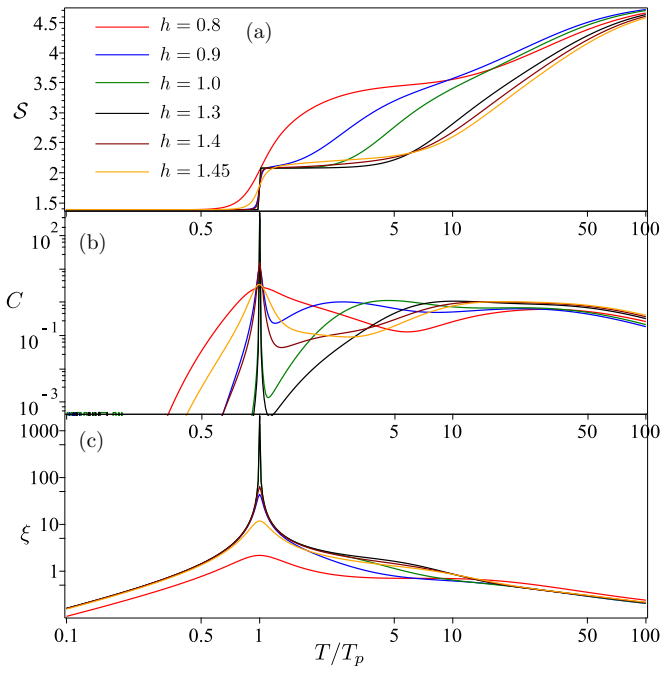

FIG. 9. (a) Entropy $\mathcal{S}$, (b) specific heat C, and (c) correlation length ξ as functions of temperature T/T_p, in units of the pseudocritical temperature T_p assuming fixed parameters $J_{ab} = -0.75$, $J_1 = -0.38$, and $q = 5$ for several values of the magnetic field $h = \{0.8, 0.9, 1.0, 1.3, 1.4, 1.45\}$ and corresponding pseudocritical temperatures $T_p = \{0.010\,065\,153\,487\,1, 0.014\,347\,308\,824\,4, 0.014\,426\,811\,788\,3, 0.014\,426\,897\,057\,9, 0.014\,398\,249\,768\,6, 0.013\,983\,016\,139\,5\}$, respectively.

However, there is no sudden jump in entropy at T_p, and when we magnify the entropy plot around T_p, we can see that the curve is a continuous smooth function. On the other hand, for other magnetic-field values, the sudden change of curves is clearly a smooth function (not shown). It is worth mentioning that for $T < T_p$, the system mostly resembles the FR_1 phase with residual entropy $\mathcal{S} = \ln(q-1) = \ln(4)$, while for $T > T_p$ the system behaves somewhat similarly to the FR_2 phase, with residual entropy $\mathcal{S} \approx \ln[2(q-1)] = \ln(8)$. This effect is more evident for magnetic fields in the range of $1 \lesssim h \lesssim 1.3$.

2. Specific heat

In Fig. 9(b) we plot specific heat C as a function of temperature T/T_p, in units of pseudocritical temperature T_p. We consider the same set of parameters as in Fig. 9(a) and each colored curve corresponds to the legend in Fig. 9(a). The anomalous behavior manifests clearly for magnetic fields in the range of $1 \lesssim h \lesssim 1.3$, where we observe a very intense sharp peak around T_p or $T/T_p = 1$, which looks like a second-order phase transition. However, there is no divergence at T_p. For other values of magnetic field, this peak becomes broader and less intense. This sharp peak around T_p evidently signals the limit between the FR_1 phase and FR_2 phase, as discussed earlier. Therefore, the plots in Fig. 9 provide valuable insights into the magnetic-field-induced phase transition in the system.

3. Correlation length

In Fig. 9(c) we plot the correlation length ξ as a function of temperature T/T_p (in units of the pseudocritical temperature T_p). For simplicity and consistency with the previous figures, we consider the same set of parameters as in Fig. 9(a). Again, we observe the anomalous behavior of the correlation length around T_p, confirming the evidence of a pseudotransition at T_p. The correlation length peak is more intense when we consider an external magnetic field in the range of $1 \lesssim h \lesssim 1.3$. This peak originates when the second largest eigenvalue becomes as important as the largest eigenvalue, although it should never attain the magnitude of the largest eigenvalue. For other values of magnetic field, the peak becomes less intense. These results further support the evidence of a magnetic-field-induced phase transition in the system, as seen in the previous plots of specific heat and entropy. The behavior of the correlation length also provides valuable insights into the nature of this transition.

The power-law behavior of the correlation length may be analytically derived using the formula proposed in Ref. [32]. This can be achieved by manipulating the relation $\xi = 1/\ln(\frac{\lambda_1}{\lambda_2})$. Utilizing the effective Boltzmann factors from (6) and (7), we can express the correlation length as

$$\xi(\tau) = c_\xi |\tau|^{-1} + O(\tau^2), \tag{32}$$

where

$$c_\xi = \frac{1}{\tilde{w}_1 T_p} \left| \frac{\partial[w_1(\beta) - w_{-1}(\beta)]}{\partial \beta} \right|_{\beta=\beta_p} \tag{33}$$

and $\tau = (T_p - T)/T_p$ with $\tilde{w}_1 = w_1(\beta_p)$.

It is worth mentioning that the power-law behavior is only valid for the ascending and descending parts of the sharp peak, but it is not valid around the top or far from the ascending and descending regions. Specifically, for our case, the range of validity is $-0.5 \lesssim \tau < 0$ and $0 < \tau \lesssim 0.9$.

4. Magnetization

In Fig. 10(a) we plot the magnetization m_c as a function of temperature T/T_p, in units of pseudocritical temperature T_p. We consider the same fixed parameter set as in Fig. 9 for comparison purposes. It is evident that for $T < T_p$, the magnetization m_c is almost negligible, indicating that almost none of the spin components are in the first component of spin. Suddenly, the magnetization increases rapidly and reaches a saturated value at $T/T_p \approx 4$, indicating that the spins are almost fully ordered. For higher temperatures, the spins gradually become randomly oriented. This behavior is more pronounced for the magnetic-field range of $1 \lesssim h \lesssim 1.3$, while for other values of magnetic field, the magnetization m_c shows a smooth curve with an enhanced magnetization slightly above T_p. Similarly, in Fig. 10(b) we present the magnetization m_{ab} as a function of temperature in units of T_p. In this case, the magnetization m_{ab} is well behaved and most of the particle's spin components are configured in the FR_1 phase. For $1 \lesssim T/T_p \lesssim 4$, the spin of the system is roughly configured in the FR_2 phase and then increases slightly. However, this peak disappears when the magnetic field satisfies the condition of $h \lesssim 1$ and $h \gtrsim 1.3$. As the temperature increases further, the magnetization decreases asymptotically.

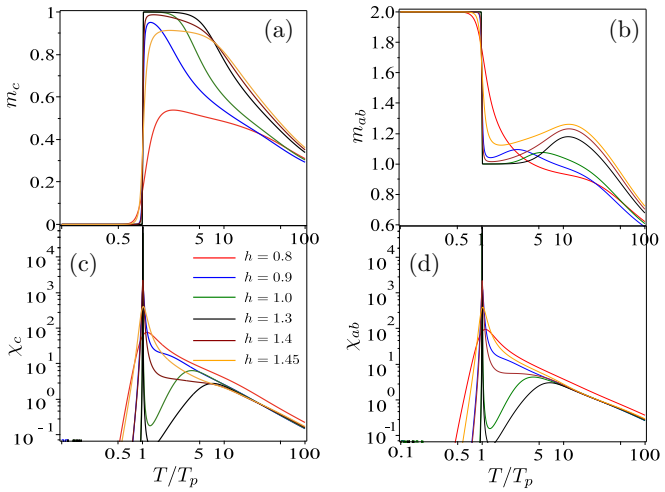

FIG. 10. (a) and (b) Magnetization and (c) and (d) magnetic susceptibility as functions of temperature T/T_p, in units of pseudocritical temperature T_p, assuming the values considered in Fig. 9. (a) Corresponds to the magnetization of nodal spins m_c and (c) shows the corresponding magnetic field.

5. Magnetic susceptibility

In Fig. 10(c) we present the nodal spin magnetic susceptibility χ_c as a function of temperature T/T_p, where we use the same set of parameters as in Figs. 10(a) and 10(b) for ease of comparison. In the range of magnetic field $1 \lesssim h \lesssim 1.3$, the χ_c peak is very sharp around $T/T_p = 1$, and a second broader peak appears at higher temperatures, which vanishes when the peak at T_p decreases. For other intervals of magnetic field, the magnetic susceptibility exhibits less intense and broader peaks around $T/T_p \approx 1$, and when the peak becomes less pronounced, the second peak disappears as well. Similarly, in Fig. 10(d) we report the magnetic susceptibility χ_{ab} as a function of temperature T/T_p. For magnetic fields $1 \lesssim h \lesssim 1.3$, the intense sharp peak delimits the boundary between quasiphases qFR_1 and qFR_2, accompanied by a second broader peak at higher temperatures. However, for other intervals of magnetic field, the intense sharp peak decreases and gradually disappears and at the same time the second broad peak vanishes as well.

To summarize our results, it is important to note that while the transfer matrix of most models exhibiting pseudotransitions is typically reduced to a 2×2 matrix as shown in Ref. [32], our transfer matrix can in principle be significantly larger, depending on the values of q. This contrasts with what was previously discussed in [32]. However, both the largest and the second-largest eigenvalues share the same structure as those of a typical 2×2 transfer matrix. In the thermodynamic limit, all other eigenvalues become irrelevant. Therefore, it is worth mentioning that pseudotransitions adhere to the same universality properties outlined in Ref. [32].

V. CONCLUSION

Here we explored the q-state Potts model on a diamond chain in order to study the zero-temperature phase transitions and thermodynamic properties. The q-state Potts model on a diamond chain exhibits intriguing behavior, due to discrete states assembled on a diamond chain structure, which exhibits several unusual features such as various possible alignments of magnetic moments.

The three-state Potts model on a diamond chain presents peculiar characteristics, around the zero-temperature FM_1-FM_2 phase transition and FR_5 and $\mathrm{FR}_5 + \mathrm{FR}_6$, such as the absence of residual entropy at the phase boundary. Thermodynamic quantities such as entropy, internal energy, and specific heat remain unaffected by this phase transition, even at significantly low temperatures, while magnetic properties such as correlation length, magnetization, and magnetic susceptibility offer evidence of a zero-temperature phase transition at finite temperatures when the magnetic field is varied. These findings highlight the intricate nature of the q-state Potts model on a diamond chain and contribute to our understanding of complex systems in diverse scientific disciplines.

Furthermore, we conducted an analysis of the q-state Potts model, primarily independent of the specific value of q, but for illustrative purposes we chose $q = 5$. Our exploration centered around the phase boundaries FR_1 and FR_2, where certain anomalous properties become more pronounced in low-temperature regions. This is due to residual entropy, which reveals unusual frustrated regions at zero-temperature phase transitions. Phase boundaries featuring nontrivial phase transitions demonstrate anomalous thermodynamic properties, including a sharp entropy alteration as a function of temperature, resembling a first-order jump of entropy without an actual discontinuity. Similarly, second-order derivatives of the free energy, such as specific heat and magnetic susceptibility, present distinct peaks akin to those found in second-order phase transition divergences, but without any singularities. The correlation length also exhibits analogous behavior at the pseudocritical temperature, marked by a sharp and robust peak that could be easily misinterpreted as true divergence. It is worth noting that, although the ground-state phase diagram shows several frustrated phases and many boundaries, only for the state near the FR_1-FR_2 boundary is there a pseudotransition at a finite temperature. This is a good demonstration of the predictive power of the criterion for pseudotransitions formulated earlier [12,13].

The pseudocritical transitions observed at the phase boundaries offer valuable insights into the interplay between temperature and magnetic field in inducing phase transitions. These findings contribute to a deeper understanding of statistical physics and phase transitions and have implications in various scientific disciplines. Further investigations into this model can open up new avenues for exploring the dynamics of complex systems and phase transitions, enriching the field of condensed matter physics.

ACKNOWLEDGMENTS

The work was partly supported by the Ministry of Science and Higher Education of the Russian Federation (Ural Federal University Program of Development within the Priority-2030 Program) and the Brazilian agencies CNPq and FAPEMIG.

APPENDIX A: DECORATION TRANSFORMATION FOR THE q-STATE POTTS MODEL

The decoration transformation [33–36] has been widely used in Ising models and Ising-Heisenberg models. In this Appendix we apply the decoration transformation mapping to transform the q-state Potts model on a diamond chain to an effective one-dimensional Potts-Zimm-Bragg model, as considered in Ref. [31].

To study the thermodynamics of the Hamiltonian (1), we need to obtain the partition function using transfer matrix techniques. The elements of the transfer matrix are commonly known as Boltzmann factors,

$$w\left(\sigma_1^c,\sigma_2^c\right)=\mathrm{e}^{(\beta h_1/2(\delta_{\sigma_1^c,1}+\delta_{\sigma_2^c,1})}\times\sum_{\sigma^a,\sigma^b=1}^{q}\left(\mathrm{e}^{\beta J_{ab}\delta_{\sigma^a,\sigma^b}+\beta h_2(\delta_{\sigma^a,1}+\delta_{\sigma^b,1})}\times\mathrm{e}^{\beta J_1(\delta_{\sigma_1^c,\sigma^a}+\delta_{\sigma_1^c,\sigma^b}+\delta_{\sigma^a,\sigma_2^c}+\delta_{\sigma^b,\sigma_2^c})}\right). \tag{A1}$$

The summation in (A1) can be expressed as

$$\sum_{\sigma^a,\sigma^b}^{q}\cdots=\left(\sum_{\sigma^a=1}^{q}\mathrm{e}^{\beta[J_1(\delta_{\sigma_1^c,\sigma^a}+\delta_{\sigma^a,\sigma_2^c})+h_2\delta_{\sigma^a,1}]}\right)^2+(y-1)\sum_{\sigma^a=1}^{q}\mathrm{e}^{2\beta[J_1(\delta_{\sigma_1^c,\sigma^a}+\delta_{\sigma^a,\sigma_2^c})+h_2\delta_{\sigma^a,1}]}, \tag{A2}$$

where we are using the notation

$$\mathrm{e}^{\beta J_{ab}\delta_{\sigma_i^a,\sigma_i^b}}=1+(y-1)\delta_{\sigma_i^a,\sigma_i^b}, \tag{A3}$$

with $y=\mathrm{e}^{\beta J_{ab}}$. Thus the Boltzmann factor (A1) can be simplified after some algebraic manipulation

$$w\left(\sigma_1^c,\sigma_2^c\right)=\nu_0+\nu_1\delta_{\sigma_1^c,\sigma_2^c}+\nu_2\delta_{\sigma_1^c,1}\delta_{1,\sigma_2^c}+\nu_3\left(\delta_{\sigma_1^c,1}+\delta_{1,\sigma_2^c}\right) \tag{A4}$$

by using the notation expressed by the simple expressions

$$\nu_0=t_2, \tag{A5}$$

$$\nu_1=d_2-t_2, \tag{A6}$$

$$\nu_2=d_1-d_2-2(t_1-t_2), \tag{A7}$$

$$\nu_3=t_1-t_2, \tag{A8}$$

where we have denoted the Boltzmann factors by $w(1,1)=d_1$, $w(\mu,\mu)=d_2$, $w(1,\mu)=t_1$, and $w(\mu,\mu')=t_2$, with μ and μ' taking values $\{2,3,\ldots,q\}$. On the other hand, based on the Hamiltonian considered in Ref. [31], let us write the effective one-dimensional Potts-Zimm-Bragg model, whose Hamiltonian has the form

$$\mathsf{H}=-\sum_{i=1}^{N}\left(K_0+K\delta_{\sigma_i^c,\sigma_{i+1}^c}+K_1\delta_{\sigma_i^c,1}\delta_{1,\sigma_{i+1}^c}+h\delta_{\sigma_i^c,1}\right), \tag{A9}$$

where K_0, K, K_1, and h must be considered as the effective parameters. Therefore, the corresponding Boltzmann factors of the effective model becomes

$$\mathsf{w}\left(\sigma_1^c,\sigma_2^c\right)=\mathrm{e}^{\beta[K_0+K\delta_{\sigma_1^c,\sigma_2^c}+K_1\delta_{\sigma_1^c,1}\delta_{1,\sigma_2^c}+(h/2)(\delta_{\sigma_1^c,1}+\delta_{1,\sigma_2^c})]}. \tag{A10}$$

Using the decoration transformation, we can impose the condition $w(\sigma_1^c,\sigma_2^c)=\mathsf{w}(\sigma_1^c,\sigma_2^c)$. This results in four nonequivalent algebraic equations that allow us to determine the four unknown effective parameters of the Hamiltonian (A9) by solving the system of equations, which results in

$$K_0=\frac{1}{\beta}\ln[w(\mu,\mu')]=\frac{1}{\beta}\ln(t_2), \tag{A11}$$

$$K=\frac{1}{\beta}\ln\left(\frac{w(\mu,\mu)}{w(\mu,\mu')}\right)=\frac{1}{\beta}\ln\left(\frac{d_2}{t_2}\right), \tag{A12}$$

$$K_1=\frac{1}{\beta}\ln\left(\frac{w(1,\mu)}{w(\mu,\mu')}\right)=\frac{1}{\beta}\ln\left(\frac{t_1}{t_2}\right), \tag{A13}$$

$$h=\frac{2}{\beta}\ln\left(\frac{w(1,1)}{w(\mu,\mu')}\right)=\frac{2}{\beta}\ln\left(\frac{d_1}{t_2}\right). \tag{A14}$$

This transformation maps the diamond chain Potts model (1) on an effective one-dimensional Potts-Zimm-Bragg model [31].

APPENDIX B: APPLICATION OF MARKOV CHAIN THEORY

It is possible to construct a mapping of our one-dimensional model to some Markov chain if we take as the entries of a transition matrix $P_{\alpha\gamma}$ the conditional probabilities $P(\gamma|\alpha)$ of the state $\gamma=|^{\xi_{i+1}}_{\eta_{i+1}}\zeta_{i+1}\rangle$ in the $(i+1)$th cell, given that the ith cell is in the state $\alpha=|^{\xi_i}_{\eta_i}\zeta_i\rangle$. Conditional probabilities are determined from the Bayes formula $P(\alpha\gamma)=P(\alpha)P(\gamma|\alpha)$, where in turn

$$P(\alpha)=\langle\Delta_{i,\alpha}\rangle, \tag{B1}$$

$$P(\alpha\gamma)=\langle\Delta_{i,\alpha}\Delta_{i+1,\gamma}\rangle, \tag{B2}$$

with $\Delta_{i,\alpha}$ a projector on the α state for the ith cell. Using the transfer matrix V, built on the states α, we find

$$\langle\Delta_{i,\alpha}\rangle=\lim_{N\to\infty}\frac{\mathrm{Tr}(V^{i-1}\Delta_{i,\alpha}V^{N-i+1})}{\mathrm{Tr}(V^N)}=\lim_{N\to\infty}\frac{\sum_k\langle\alpha|\lambda_k\rangle\lambda_k^N\langle\lambda_k|\alpha\rangle}{\sum_k\lambda_k^N}=\langle\alpha|\lambda_1\rangle\langle\lambda_1|\alpha\rangle, \tag{B3}$$

$$\langle\Delta_{i,\alpha}\Delta_{i+1,\gamma}\rangle=\frac{V_{\alpha\gamma}}{\lambda_1}\langle\gamma|\lambda_1\rangle\langle\lambda_1|\alpha\rangle. \tag{B4}$$

Here λ_1 is the maximum eigenvalue of the transfer matrix V. For a positive matrix, the coefficients $v_\alpha=\langle\alpha|\lambda_1\rangle$ can be chosen to be positive, according to Perron's theorem [37]. Assuming that

$$P_{\alpha\gamma}=P(\gamma|\alpha)=\frac{\langle\Delta_{i,\alpha}\Delta_{i+1,\gamma}\rangle}{\langle\Delta_{i,\alpha}\rangle}, \tag{B5}$$

we obtain

$$P_{\alpha\gamma}=\frac{V_{\alpha\gamma}v_\gamma}{\lambda_1 v_\alpha}. \tag{B6}$$

The stochastic properties of the matrix $P_{\alpha\gamma}$ are checked directly:

$$\sum_\gamma P_{\alpha\gamma}=\frac{1}{\lambda_1 v_\alpha}\sum_\gamma V_{\alpha\gamma}v_\gamma=1. \tag{B7}$$

Equation (B6) for constructing a transition matrix is known in the theory of non-negative matrices [37], but the expression (B5) reveals its physical content for our model. This allows us to use the results of a very advanced field of mathematics, the theory of Markov chains. The state of the system is determined by the stationary probability vector $\mathbf{w}$ of the Markov chain, which can be found from the equations

$$\sum_{\alpha} w_\alpha P_{\alpha\gamma} = w_\gamma, \quad \sum_{\alpha} w_\alpha = 1. \tag{B8}$$

Using (B3), we can check that $w_\alpha = P(\alpha)$, and if the transfer matrix V is chosen to be symmetric, then $w_\alpha = v_\alpha^2$. For the magnetizations, we obtain the expressions

$$m_c = \mathbf{w}\mathbf{m}_c, \quad m_{ab} = \mathbf{w}\mathbf{m}_{ab}, \tag{B9}$$

where the αth component of the vector $\mathbf{m}$ equals the corresponding magnetization for the state α.

The calculation of the transition matrix P involves finding the maximum eigenvalue λ_1 of the transfer matrix V, the dimension of which for our model is q^3. However, the dimension of the matrices can be reduced using the lumpability method for reducing the size of the state space of Markov chain [38]. We divide the original set of m states into M groups and find the lumped transition matrix. Formally, this can be done using matrices $L_{A\alpha}$ and $R_{\gamma G}$ ($\alpha, \gamma = 1, \ldots, m$ and $A, G = 1, \ldots, M$),

$$P_{AG} = \sum_{\alpha\gamma} L_{A\alpha} P_{\alpha\gamma} R_{\gamma G}, \tag{B10}$$

where $R_{\gamma G} = 1$ if the state γ belongs to the group with the number G and $R_{\gamma G} = 0$ otherwise; $L_{A\alpha} = 1/\dim(A)$ if the state α belongs to the group with the number A consisting of $\dim(A)$ elements and $L_{A\alpha} = 0$ otherwise.

In our problem, it is natural to divide $m = q^3$ states into phases (19)–(23). Also, to complete the set of states, it is necessary to supplement this list with two phases FR′ and FR″, the states for which have the form

$$|\mathrm{FR}'\rangle = \prod_i \left|\left[{}^{1}_{\mu}\right]\mu\right\rangle_i, \quad |\mathrm{FR}''\rangle = \prod_i \left|{}^{\mu_i}_{\mu_i} 1\right\rangle_i. \tag{B11}$$

The energy and entropy at zero temperature have the values

$$\varepsilon_0 = -(2J_1 + h), \quad \mathcal{S}_0 = \ln 2 \quad \text{for FR}', \tag{B12}$$

$$\varepsilon_0 = -(J_{ab} + h), \quad \mathcal{S}_0 = \ln(q-1) \quad \text{for FR}''. \tag{B13}$$

The states FR′ and FR″ are not represented in the phase diagrams of the ground state in Figs. 3 and 4 by their own domains, but appear as impurities in mixed states at the phase boundaries. Thus, for any $q > 3$ the matrix P_{AG} will have dimension $M = 11$, and $M = 10$ for $q = 3$.

The equilibrium state of the system will correspond to a stationary probability vector for the lumped Markov chain,

$$\sum_{A} w_A P_{AG} = w_G, \quad \sum_{A} w_A = 1, \tag{B14}$$

and the expressions for magnetizations will not formally change. The lumpability (B10) can also be applied to the transfer matrix V, if we are only interested in its maximum eigenvalue. Indeed, the matrix V is non-negative, so according

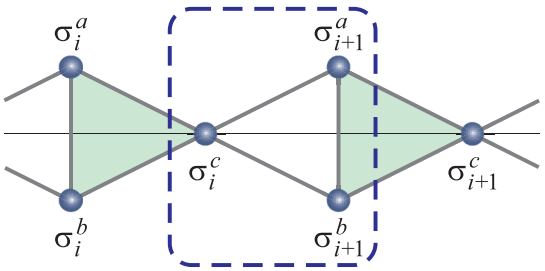

FIG. 11. Illustration of the interface between the ith and $(i+1)$th cells of the diamond chain.

to the Perron-Frobenius theorem [37]

$$\lambda_1 = \max_{(v\geqslant 0)} \min_{1\leqslant\alpha\leqslant m} \frac{\sum_\beta V_{\alpha\gamma} v_\gamma}{v_\alpha}. \tag{B15}$$

Since the matrix R sums the matrix elements for states from the group and the matrix L removes duplicate rows, the value of λ_1 in Eq. (B15) will not change after the lumpability.

This computational scheme is greatly simplified for the ground state. We will count the energy of the system from the energy of the ground state $E_0 = N\varepsilon_0$. If $T = 0$, then for all states with energy higher than ε_0 we get $V_{\alpha\gamma} = 0$. A pair of states $\alpha = |{}^{\xi_\alpha}_{\eta_\alpha}\zeta_\alpha\rangle$ and $\gamma = |{}^{\xi_\gamma}_{\eta_\gamma}\zeta_\gamma\rangle$ with energy equal to ε_0 will be called allowable if the state of the interface $|{}^{\xi_\gamma}_{\eta_\gamma}\zeta_\alpha\rangle$ also has energy ε_0 (see Fig. 11). For the allowable pair of states, we get $V_{\alpha\gamma} = 1$; otherwise $V_{\alpha\gamma} = 0$. For the lumped matrix, the nonzero matrix elements V_{AG} will be equal to the number of allowable pairs for any state α from the group A and all states from the group G. As a result, the dimension of a block with nonzero matrix elements will in most cases be less than M.

It can also be shown that for the ground state the entropy per cell can be calculated as

$$\mathcal{S}_0 = \ln \lambda_1, \tag{B16}$$

where λ_1 is the maximum eigenvalue of the matrix $V_{\alpha\gamma}$ (or V_{AG}) at $T = 0$. For a cyclic closed sequence, the probability of the state $(\alpha_1 \cdots \alpha_N \alpha_1)$ has the following form [39]:

$$\begin{aligned} P(\alpha_1 \cdots \alpha_N \alpha_1) &= P(\alpha_1|\alpha_2) P(\alpha_1|\alpha_2) \cdots P(\alpha_N|\alpha_1) \\ &= \prod_{\alpha\gamma} P(\alpha|\gamma)^{NP(\alpha\gamma)} = p_0^N. \end{aligned} \tag{B17}$$

In the ground state, the equation $\mathcal{S}_0 = -\ln p_0$ is valid [40]. Consider the limit of $\ln p_0$ at zero temperature. We have

$$\begin{aligned} \ln p_0 = &\sum_{\alpha} P(\alpha\alpha) \ln P(\alpha|\alpha) \\ &+ \sum_{\alpha<\gamma} P(\alpha\gamma) \ln[P(\alpha|\gamma) P(\gamma|\alpha)]. \end{aligned} \tag{B18}$$

Using Eqs. (B5) and (B6), we obtain

$$P(\alpha|\alpha) = \frac{V_{\alpha\alpha}}{\lambda_1}, \quad P(\alpha|\gamma) P(\gamma|\alpha) = \frac{V_{\alpha\gamma} V_{\gamma\alpha}}{\lambda_1^2}. \tag{B19}$$

Equation (B17) takes the form

$$\ln p_0 = \sum_{\alpha\gamma} P(\alpha\gamma) \ln V_{\alpha\gamma} - \ln \lambda_1. \tag{B20}$$

For allowable pairs $P(\alpha\gamma) \neq 0$ and $V_{\alpha\gamma} \to 1$ at $T \to 0$; hence $P(\alpha\gamma)\ln V_{\alpha\gamma} \to 0$. For the other pairs $V_{\alpha\gamma} \to 0$, and hence $P(\alpha\gamma)\ln V_{\alpha\gamma} \propto V_{\alpha\gamma}\ln V_{\alpha\gamma} \to 0$ at $T \to 0$. As a result, $\mathcal{S} \to \ln\lambda_1$ at $T \to 0$.

Example 1. Consider the ground state at the boundary between phases FR_1 and FR_4. The energies of these phases $\varepsilon_{FR_1} = -(J_{ab} + 2h)$ and $\varepsilon_{FR_4} = -J_{ab}$ become equal to $\varepsilon_0 = -J_{ab}$ if $h = 0$. The FR″ phase has the same energy. These phase states for the ith cell have the form

$$|FR_1\rangle_i = \left|{}^{1}_{1}\mu_i\right\rangle, \tag{B21}$$

$$|FR_4\rangle_i = \left|{}^{\nu_i}_{\nu_i}\mu_i\right\rangle, \tag{B22}$$

$$|FR''\rangle_i = \left|{}^{\mu_i}_{\mu_i}1\right\rangle, \tag{B23}$$

so that

$$\mathbf{m}_c = \begin{pmatrix}0\\0\\1\end{pmatrix}, \quad \mathbf{m}_{ab} = \begin{pmatrix}2\\0\\0\end{pmatrix}. \tag{B24}$$

The nonzero block of the matrix V_{AB} has the following form:

$$V = \begin{pmatrix} q-1 & (q-2)^2 & q-2 \\ q-1 & (q-2)^2 & q-2 \\ 0 & (q-1)(q-2) & q-1 \end{pmatrix}. \tag{B25}$$

Here we take into account that the interface state for FR″-FR_1 pairs has the form FM_1, with energy higher than ε_0, and for FR_1-FR″ pairs, for example, an invalid state FM_2 may also occur. Finding the maximum eigenvalue of $\lambda_1 = (q-1)^2$, we get

$$\mathcal{S}_0 = 2\ln(q-1), \quad \mathbf{v} = C\begin{pmatrix}1\\1\\1\end{pmatrix} \tag{B26}$$

and calculate the transition matrix

$$P = \frac{1}{q-1}\begin{pmatrix} 1 & \frac{(q-2)^2}{q-1} & \frac{q-2}{q-1} \\ 1 & \frac{(q-2)^2}{q-1} & \frac{q-2}{q-1} \\ 0 & q-2 & 1 \end{pmatrix} \quad \text{for } P_{AG} = \frac{V_{AG}}{\lambda_1}\frac{v_G}{v_A}. \tag{B27}$$

Finding the stationary distribution of the lumped Markov chain

$$\mathbf{w} = \frac{1}{q}\begin{pmatrix}1\\q-2\\1\end{pmatrix} \quad \text{for } P^T\mathbf{w} = \mathbf{w}, \tag{B28}$$

we calculate the magnetizations

$$m_c = \mathbf{w}\mathbf{m}_c = \frac{1}{q}, \quad m_{ab} = \mathbf{w}\mathbf{m}_{ab} = \frac{2}{q}. \tag{B29}$$

Note that without taking into account the FR″ states, the nonzero magnetization m_c at the FR_1-FR_4 phase boundary looks mysterious, since for these phases themselves $m_c = 0$. Similarly, the FR′ states contribute in a state of the FR_2-FR_3 phase boundary, where the energies of these three states are equal.

Example 2. For the ground state at the boundary between phases FR_2 and FR_6, the energies of these phases $\varepsilon_{FR_2} = -2(J_1 + h)$ and $\varepsilon_{FR_6} = -h$ become equal to $\varepsilon_0 = 2J_1$ if $h = -2J_1$. The phase FR_5 has the same energy. These phase states for the ith cell have the form

$$|FR_2\rangle_i = \left|{}^{1}_{[\mu_i}]1\right\rangle, \tag{B30}$$

$$|FR_6\rangle_i = \left|{}^{1}_{\nu_i]}\mu_i\right\rangle, \tag{B31}$$

$$|FR_5\rangle_i = \left|{}^{\mu_i}_{\nu_i}1\right\rangle \tag{B32}$$

and

$$\mathbf{m}_c = \begin{pmatrix}1\\0\\1\end{pmatrix}, \quad \mathbf{m}_{ab} = \begin{pmatrix}1\\1\\0\end{pmatrix}. \tag{B33}$$

The lumped transfer matrix

$$V = \begin{pmatrix} 2(q-1) & 2(q-1)(q-2) & (q-1)(q-2) \\ 2(q-2) & 2(q-2)^2 & 0 \\ 2(q-1) & 2(q-1)(q-2) & (q-1)(q-2) \end{pmatrix} \tag{B34}$$

has a maximum eigenvalue

$$\lambda_1 = \tfrac{1}{2}[3q^2 - 9q + 8 + \phi_1(q)], \tag{B35}$$

where

$$\phi_1(q) = \sqrt{q^4 + 2q^3 - 15q^2 + 16q}. \tag{B36}$$

We write the corresponding eigenvector

$$\mathbf{v} = C\begin{pmatrix} 1 \\ \frac{(q-2)(q^2-3q+4+\phi_1(q))}{(q-1)(3q^2-9q+8+\phi_1(q))} \\ 1 \end{pmatrix} \tag{B37}$$

and find the transition matrix

$$P = \begin{pmatrix} \frac{2(q-1)}{\lambda_1} & \frac{2(q-2)^2(\lambda_1-q^2+3q-2)}{\lambda_1^2} & \frac{(q-2)(q-1)}{\lambda_1} \\ \frac{2(q-1)}{\lambda_1-q^2+3q-2} & \frac{2(q-2)^2}{\lambda_1} & 0 \\ \frac{2(q-1)}{\lambda_1} & \frac{2(q-2)^2(\lambda_1-q^2+3q-2)}{\lambda_1^2} & \frac{(q-2)(q-1)}{\lambda_1} \end{pmatrix}. \tag{B38}$$

The stationary probabilities can be reduced to the form

$$\mathbf{w} = \frac{1}{2\phi_1(q)}\begin{pmatrix} 4(q-1) \\ \phi_1(q) + q^2 - 7q + 8 \\ \phi_1(q) - q^2 + 3q - 4 \end{pmatrix}, \tag{B39}$$

which allows us to find the magnetizations

$$m_c = \frac{\phi_1(q) - q^2 + 7q - 8}{2\phi_1(q)}, \tag{B40}$$

$$m_{ab} = \frac{\phi_1(q) + q^2 - 3q + 4}{2\phi_1(q)}. \tag{B41}$$

In this way, it is possible to obtain all the values given in Table I.

A special situation occurs at $q = 3$, when the ground-state energy has the value $\varepsilon_0 = -h$. This value has the energy of the FR_5 and FR_6 phases. At $q > 3$, the entropy of the FR_6 phase is greater than that of the FR_5 phase, so when $T > 0$, the free energy for the FR_6 phase is less than that for the FR_5 phase, and in the limit $T \to 0$ the main state is the FR_6 phase. If $q = 3$, the entropy of the FR_5 and FR_6 phases is equal to $\mathcal{S}_0 = \ln 2$. The nature of the ground state in this case can be investigated using the Markov chain method proposed above.

At a sufficiently low temperature, the state of the system is formed by phases whose energies are closest to the energy of the ground state. In the parameter range of $h > 0$, $J_1 < -h/2$, and $J_{ab} < -h$ [see Fig. 4(a)], it is natural to take into account in addition to FR_5 and FR_6 phases also neighboring phases FR_1 and FR_2. The transfer matrix with entries V_{AB}, where $A, B = FR_1, FR_2, FR_5, FR_6$, has the form

$$V = 2z\begin{pmatrix} yz & \sqrt{xyz}(1+x) & x\sqrt{yz} & \sqrt{yz}(1+x) \\ x^{5/2}\sqrt{yz} & 2x^2 z & \sqrt{xz} & 2x^{3/2}\sqrt{z} \\ x^2\sqrt{yz} & 2x^{3/2}\sqrt{z} & 1 & 2x \\ \sqrt{yz} & \sqrt{xz}(1+x) & x & 1+x \end{pmatrix}. \tag{B42}$$

Here $x = e^{\beta J_1}$, $y = e^{\beta J_{ab}}$, $z = e^{\beta h}$, and it is taken into account that $q = 3$. Explicit expressions for the maximum eigenvalue λ_1 and its eigenvector $\mathbf{v}$ have a rather cumbersome form; however, for the parameters under consideration and $\beta \gg 1$, their approximate expressions can be used:

$$\lambda_1 = 2z(1+u), \quad \mathbf{v} = C\begin{pmatrix} \sqrt{yz} \\ 2x^{3/2}\sqrt{z}/u \\ 2x/u \\ 1 \end{pmatrix}, \tag{B43}$$

where

$$u = \tfrac{1}{2}(yz + \sqrt{y^2z^2 + 8x^2 z}). \tag{B44}$$

Using these expressions in Eq. (B6) and leaving only the leading terms for $\beta \gg 1$ in the entries of the matrix V, we obtain the transition matrix

$$P = \frac{1}{1+u}\begin{pmatrix} yz & \frac{2x^2 z}{u} & \frac{2x^2}{u} & 1 \\ \frac{1}{2}uxyz & 2x^2 z & 1 & u \\ \frac{1}{2}uxyz & 2x^2 z & 1 & u \\ yz & \frac{2x^2 z}{u} & \frac{2x^2}{u} & 1 \end{pmatrix}. \tag{B45}$$

In the parameter domain under consideration, the stochastic properties of this matrix remain quite accurate at $\beta \gg 1$. The qualitative difference of Markov chains generated by P at low temperature depends on the asymptotic behavior of the parameter u:

$$u \underset{\beta\gg 1}{\longrightarrow} \begin{cases} yz, & 2J_{ab} + h > 2J_1 \\ 2yz = 2x\sqrt{z}, & 2J_{ab} + h = 2J_1 \\ x\sqrt{2z}, & 2J_{ab} + h < 2J_1. \end{cases} \tag{B46}$$

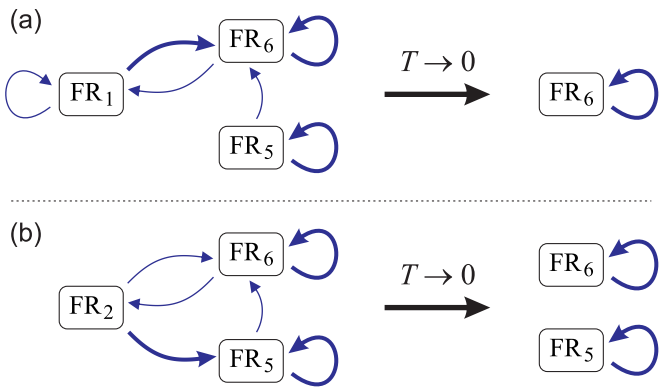

FIG. 12. Transition graphs of Markov chains at $q = 3$, $h > 0$, $2J_1 < -h$, $J_{ab} < -h$, and low temperature for (a) $2J_{ab} + h > 2J_1$ and (b) $2J_{ab} + h < 2J_1$.

Consider the case of $2J_{ab} + h > 2J_1$. Under this condition, the following inequalities will be true: $x^2 \ll x^2 z \ll yz$ and $uxyz \ll yz$. For clarity, we leave in the matrix P only entries of order 1 and the first order of smallness and replace matrix elements of higher orders of smallness with zeros. As a result, the transition matrix takes the form

$$P = \begin{pmatrix} a_1 & 0 & 0 & 1-a_1 \\ 0 & 0 & 1-a_1 & a_1 \\ 0 & 0 & 1-a_1 & a_1 \\ a_1 & 0 & 0 & 1-a_1 \end{pmatrix}, \quad a_1 = yz. \tag{B47}$$

The transition graph of this Markov chain is shown in Fig. 12(a). The state FR_2 in this case is transient and is omitted for simplicity. Thin and thick lines correspond to the transition probabilities a_1 and $1 - a_1$. The stationary state contains an exponentially small admixture of the FR_1 phase and in the limit of $T \to 0$ becomes a pure FR_6 phase:

$$\mathbf{w} = \begin{pmatrix} a_1 \\ 0 \\ 0 \\ 1-a_1 \end{pmatrix} \underset{T\to 0}{\longrightarrow} \begin{pmatrix} 0 \\ 0 \\ 0 \\ 1 \end{pmatrix}. \tag{B48}$$

If $2J_{ab} + h > 2J_1$, when $u \approx x\sqrt{2z}$, the estimates hold $uxyz \ll yz \ll u$, $x^2 \ll u$, and $2x^2 z/u \approx u$. Replacing exponentially small entries with zeros, we get the transition matrix

$$P = \begin{pmatrix} 0 & a_2 & 0 & 1-a_2 \\ 0 & 0 & 1-a_2 & a_2 \\ 0 & 0 & 1-a_2 & a_2 \\ 0 & a_2 & 0 & 1-a_2 \end{pmatrix}, \quad a_2 = x\sqrt{2z}. \tag{B49}$$

The corresponding graph without the transient state FR_1 is shown in Fig. 12(b). Thin and thick lines correspond to the transition probabilities a_2 and $1 - a_2$, respectively. The stationary state in this case contains an exponentially small admixture of the FR_2 phase and at $T \to 0$ transforms into a mixture of independent phases FR_5 and FR_6 having equal

fractions:

$$\mathbf{w} = \tfrac{1}{2}\begin{pmatrix} 0 \\ a_2 \\ 1-a_2 \\ 1 \end{pmatrix} \xrightarrow[T\to 0]{} \tfrac{1}{2}\begin{pmatrix} 0 \\ 0 \\ 1 \\ 1 \end{pmatrix}. \tag{B50}$$

It is this state that is designated as $\mathrm{FR}_5 + \mathrm{FR}_6$ in Fig. 4(a).

On the boundary $2J_{ab} + h = 2J_1$, similar considerations give a transition matrix

$$P = \begin{pmatrix} a_3 & a_3 & 0 & 1-2a_3 \\ 0 & 0 & 1-2a_3 & a_3 \\ 0 & 0 & 1-2a_3 & a_3 \\ a_3 & a_3 & 0 & 1-2a_3 \end{pmatrix}, \quad a_3 = x\sqrt{z} = yz. \tag{B51}$$

The stationary state in this case transforms at $T \to 0$ into a mixture of independent phases FR_5 and FR_6 with a ratio of fractions of $\frac{1}{2}$:

$$\mathbf{w} = \tfrac{1}{3}\begin{pmatrix} 2a_3 \\ 2a_3 \\ 1-2a_3 \\ 2-2a_3 \end{pmatrix} \xrightarrow[T\to 0]{} \tfrac{1}{3}\begin{pmatrix} 0 \\ 0 \\ 1 \\ 2 \end{pmatrix}. \tag{B52}$$

At $h < 0$, similar results for the composition of the phases of the ground state, shown in Fig. 4(b), can be obtained by taking into account the mixing of the FR_5 and FR_6 phase states of neighboring phases FR_3 and FR_4. A special composition of the ground state also occurs at $h = 0$ in the region of phases FR_6 and $\mathrm{FR}_5 + \mathrm{FR}_6$ in Figs. 4(d) and 4(f). The stationary state at $T = 0$ on the line $h = 0$ is a mixture of FR_5 and FR_6 with a ratio of fractions of $\frac{1}{2}$.

[1] F. Y. Wu, The Potts model, Rev. Mod. Phys. **54**, 235 (1982).

[2] R. J. Baxter, *Exactly Solved Models in Statistical Mechanics* (Academic, London, 1982).

[3] O. Bernardi and M. Bousquet-Mélou, Counting colored planar maps: Algebraicity results, J. Comb. Theory, Ser. B **101**, 315 (2011).

[4] D. P. Landau and K. Binder, *A Guide to Monte Carlo Simulations in Statistical Physics*, 5th ed. (Cambridge University Press, Cambridge, 2020).

[5] J. Torrico, M. Rojas, S. M. de Souza, O. Rojas, and N. S. Ananikian, Pairwise thermal entanglement in the Ising-XYZ diamond chain structure in an external magnetic field, Europhys. Lett. **108**, 50007 (2014).

[6] J. Torrico, M. Rojas, S. de Souza, and O. Rojas, Zero temperature non-plateau magnetization and magnetocaloric effect in an Ising-XYZ diamond chain structure, Phys. Lett. A **380**, 3655 (2016).

[7] L. Gálisová and J. Strečka, Vigorous thermal excitations in a double-tetrahedral chain of localized Ising spins and mobile electrons mimic a temperature-driven first-order phase transition, Phys. Rev. E **91**, 022134 (2015).

[8] O. Rojas, J. Strečka, and S. de Souza, Thermal entanglement and sharp specific-heat peak in an exactly solved spin-1/2 Ising-Heisenberg ladder with alternating Ising and Heisenberg inter–leg couplings, Solid State Commun. **246**, 68 (2016).

[9] J. Strečka, R. C. Alécio, M. L. Lyra, and O. Rojas, Spin frustration of a spin-1/2 Ising–Heisenberg three-leg tube as an indispensable ground for thermal entanglement, J. Magn. Magn. Mater. **409**, 124 (2016).

[10] S. de Souza and O. Rojas, Quasi-phases and pseudo-transitions in one-dimensional models with nearest neighbor interactions, Solid State Commun. **269**, 131 (2018).

[11] I. Carvalho, J. Torrico, S. de Souza, O. Rojas, and O. Derzhko, Correlation functions for a spin-$\frac{1}{2}$ Ising-XYZ diamond chain: Further evidence for quasi-phases and pseudo-transitions, Ann. Phys. (NY) **402**, 45 (2019).

[12] O. Rojas, Residual Entropy and low temperature pseudo-transition for one-dimensional models, Acta Phys. Pol. A **137**, 933 (2020).

[13] O. Rojas, A conjecture on the relationship between critical residual entropy and finite temperature pseudo-transitions of one-dimensional models, Braz. J. Phys. **50**, 675 (2020).

[14] A. Honecker, S. Hu, R. Peters, and J. Richter, Dynamic and thermodynamic properties of the generalized diamond chain model for azurite, J. Phys.: Condens. Matter **23**, 164211 (2011).

[15] L. Čanová, J. Strečka, and M. Jaščur, Geometric frustration in the class of exactly solvable Ising–Heisenberg diamond chains, J. Phys.: Condens. Matter **18**, 4967 (2006).

[16] B. Lisnii, Spin-1/2 asymmetric diamond Ising-Heisenberg chain, Ukr. J. Phys. **56**, 1237 (2011).

[17] O. Rojas, S. M. de Souza, V. Ohanyan, and M. Khurshudyan, Exactly solvable mixed-spin Ising-Heisenberg diamond chain with biquadratic interactions and single-ion anisotropy, Phys. Rev. B **83**, 094430 (2011).

[18] J. S. Valverde, O. Rojas, and S. M. de Souza, Phase diagram of the asymmetric tetrahedral Ising-Heisenberg chain, J. Phys.: Condens. Matter **20**, 345208 (2008).

[19] O. Rojas and S. de Souza, Spinless fermion model on diamond chain, Phys. Lett. A **375**, 1295 (2011).

[20] K. C. Rule, A. U. B. Wolter, S. Süllow, D. A. Tennant, A. Brühl, S. Köhler, B. Wolf, M. Lang, and J. Schreuer, Nature of the spin dynamics and $\frac{1}{3}$ magnetization plateau in azurite, Phys. Rev. Lett. **100**, 117202 (2008).

[21] H. Kikuchi, Y. Fujii, M. Chiba, S. Mitsudo, T. Idehara, T. Tonegawa, K. Okamoto, T. Sakai, T. Kuwai, and H. Ohta, Experimental observation of the $\frac{1}{3}$ magnetization plateau in the diamond-chain compound $Cu_3(CO_3)_2(OH)_2$, Phys. Rev. Lett. **94**, 227201 (2005).

[22] H. Kikuchi, Y. Fujii, M. Chiba, S. Mitsudo, T. Idehara, T. Tonegawa, K. Okamoto, T. Sakai, T. Kuwai, K. Kindo, A. Matsuo, W. Higemoto, K. Nishiyama, M. Horvatić, and C. Bertheir, Magnetic properties of the diamond chain compound $Cu_3(CO_3)_2(OH)_2$, Prog. Theor. Phys. Suppl. **159**, 1 (2005).

[23] N. S. Ananikian, L. N. Ananikyan, L. A. Chakhmakhchyan, and O. Rojas, Thermal entanglement of a spin-1/2 Ising-Heisenberg model on a symmetrical diamond chain, J. Phys.: Condens. Matter **24**, 256001 (2012).

[24] L. Chakhmakhchyan, N. Ananikian, L. Ananikyan, and Č. Burdík, Thermal entanglement of the spin-1/2 diamond chain, J. Phys.: Conf. Ser. **343**, 012022 (2012).

[25] P. Sarkanych, Y. Holovatch, and R. Kenna, Exact solution of a classical short-range spin model with a phase transition in one dimension: The Potts model with invisible states, Phys. Lett. A **381**, 3589 (2017).

[26] B. H. Zimm and J. K. Bragg, Theory of the phase transition between helix and random coil in polypeptide chains, J. Chem. Phys. **31**, 526 (1959).

[27] A. V. Badasyan, A. Giacometti, Y. S. Mamasakhlisov, V. F. Morozov, and A. S. Benight, Microscopic formulation of the Zimm-Bragg model for the helix-coil transition, Phys. Rev. E **81**, 021921 (2010).

[28] N. S. Ananikyan, S. A. Hajryan, E. S. Mamasakhlisov, and V. F. Morozov, Helix-coil transition in polypeptides: A microscopical approach, Biopolymers **30**, 357 (1990).

[29] A. Badasyan, A. Giacometti, R. Podgornik, Y. Mamasakhlisov, and V. Morozov, Helix-coil transition in terms of Potts-like spins, Eur. Phys. J. E **36**, 46 (2013).

[30] S. Tonoyan, D. Khechoyan, Y. Mamasakhlisov, and A. Badasyan, Statistical mechanics of DNA-nanotube adsorption, Phys. Rev. E **101**, 062422 (2020).

[31] Y. Panov and O. Rojas, Unconventional low-temperature features in the one-dimensional frustrated q-state Potts model, Phys. Rev. E **103**, 062107 (2021).

[32] O. Rojas, J. Strečka, M. L. Lyra, and S. M. de Souza, Universality and quasicritical exponents of one-dimensional models displaying a quasitransition at finite temperatures, Phys. Rev. E **99**, 042117 (2019).

[33] M. E. Fisher, Transformations of Ising models, Phys. Rev. **113**, 969 (1959).

[34] I. Syozi, The statistics of honeycomb and triangular lattice. II, Prog. Theor. Phys. **5**, 341 (1950).

[35] O. Rojas, J. Valverde, and S. de Souza, Generalized transformation for decorated spin models, Physica A **388**, 1419 (2009).

[36] O. Rojas and S. M. de Souza, Direct algebraic mapping transformation for decorated spin models, J. Phys. A: Math. Theor. **44**, 245001 (2011).

[37] F. R. Gantmacher and F. R. Gantmacher, *The Theory of Matrices* (American Mathematical Society, Providence, 2000).

[38] J. G. Kemeny and J. L. Snell, *Finite Markov Chains* (Springer, New York, 1976).

[39] Y. Panov, Local distributions of the 1D dilute Ising model, J. Magn. Magn. Mater. **514**, 167224 (2020).

[40] Y. Panov, Residual entropy of the dilute Ising chain in a magnetic field, Phys. Rev. E **106**, 054111 (2022).